

## Effect of nano-structuration and compounding of YSZ APS TBCs with different thickness on coating performance in thermal shock conditions

A. Ashofteh<sup>a,\*</sup>, M. Mosavi Mashhadi<sup>a</sup> and A. Amadeh<sup>b</sup>

<sup>a</sup> Department of Mechanical Engineering, College of Engineering, University of Tehran, Tehran, Iran

<sup>b</sup> Department of Metallurgy and Materials Engineering, College of Engineering, University of Tehran, Tehran, Iran

### ARTICLE INFO

#### Article history:

Received: 07 Aug. 2017

Accepted: 18 Sep. 2017

#### Keywords:

Thermal barrier coating

Thermal Shock

Nano-YSZ

YSZ

CSZ

### ABSTRACT

Effect of nano-structuration and compounding of YSZ APS TBCs investigated on coating behavior in thermal shock conditions. The coatings were applied on Inconel 738 discs with three different thickness per powder. In order to harmonize the results from the samples, performance factor is defined as a criterion that in the starting of the activity has an amount of about 100 and is reduced after the damage begins. The results revealed that the growth of damage in the YSZ class is almost linear, and this behavior is observed in all samples. The thick TGO in this class shows its high oxygen permeability, and the type of damage indicates that its location is near the TGO region. The nano-structured YSZ class has a very good performance and through an interesting phenomenon, the slope of the damage growth diagrams is decreasing with time. The obvious thing about the CSZ class microstructure is the presence of horizontal and vertical cracks and its dense structure. In this class, the main location of damage is through the coating and after the beginning of damage, its curve has grown with a high rate. The best performance among all samples belongs to the nano-structured YSZ, which due to the presence of nano-zones, has a higher toughness and ability to endure more cycles.

### 1. Introduction

The presence of thermal barrier coatings on high-temperature components can lead to working at higher temperature and durability in complex conditions created at high temperatures. Some of the results of using TBCs include: increasing component life and working temperature, reducing fuel consumption, increasing resistance to external particle damage and reducing fatigue and creep in parts. In general, the use of these coatings can increase the overall efficiency [1-5]. The main requirements for the development of turbines are their ability to operate more reliable at higher temperatures, and one of the tools to achieve this goals is using of TBCs [6-10].

TBCs have a multi-layered structure that apply on nickel or cobalt base super alloys substrate and main features of different layers are [11-16]:

- Bondcoat (BC): common composition of this layer is MCrAlY (m=metal, Cr: chrome, Al: aluminum and Y=yttrium) and had thickness in range 50-150  $\mu\text{m}$ . This layer has properties between ceramic (topcoat) and metal (substrate) and is rich in Al. Bondcoat protect the substrate

from oxidation and hot corrosion.

- Topcoat (TC): topcoat is the outer layer of TBC system and most common material for this layer is Ytria Stabilized Zirconia (YSZ). Thickness of TC according to the working condition and environmental situation change in range 250-600  $\mu\text{m}$ . Topcoat has low thermal conductivity and high thermal expansion coefficient (CTE); also its resistance to sintering and phase stability at the high temperatures is high. Normally TC reduce temperature 100-200 K.
- Thermally grown oxide (TGO): this layer forms between BC and TC and thicken with time. Main composition of TGO is  $\alpha\text{-Al}_2\text{O}_3$  and its thickness is in range of 0.1-10  $\mu\text{m}$ . TGO needs Al and O for growing that Al comes from BC and oxygen penetrates from atmosphere. CTE mismatch with the upper and lower layers causes a high compressive residual stresses within the coating. Researches shows that amount of damage is directly related to the thickness of this layer. YSZ has unique properties, including high CTE (close to metals)

\* Corresponding author. Tel.: +98-910-807-0521;; e-mail: [a.ashofteh@ut.ac.ir](mailto:a.ashofteh@ut.ac.ir)

and low thermal conductivity, and therefore is the main choice for using in TBCs. But this material has weaknesses such as phase change and sintering at temperatures above 1200°C and high oxygen permeability, and its performance in thermal shock conditions is also normal [17-20].

One way to improve YSZ properties is to add some compounds to it. One of these combinations is the CeO<sub>2</sub>, whose addition to the YSZ creates Ceria-ytria co-Stabilized Zirconia (CSZ). The characteristics of resulting compounds include lower thermal conductivity, better resistance to hot corrosion and higher CTE than YSZ, but the use of it will increase the rate of sintering [6, 21].

Nano-structuration of TBCs is one of the methods proposed to improve its properties. Previous studies have shown that nanostructured coatings exhibit more creep and thermal shock resistance, and have lower thermal diffusivity. To create a nanoscale coating, powders with size less than 100 nanometers should be used, which, due to their very low mass, cannot accelerate in plasma stream during spraying. Therefore, nanoparticles must be agglomerated before spraying operation. To create a nano-structured coating, the parameters must be selected in such a way that a portion of the nano-sized particles be melted and create a good bonding and others remains non-melted. If the all of the nano-particles melted, the coating would be micro-structured [22-24].

The basis of the creation of TBCs is the melting ceramic particles and applying them to the surface, and according to the high melting point of ceramics (about 2800 °C), few methods are capable of doing this. In industry, air plasma spraying (APS) and electron beam physical vapor deposition (EBPVD) are commonly used, that former being more applicable in power plants due to lower costs and the defected structure of created coating [3, 18]. In the structure of APS coatings, there are defects such as porosity and micro-cracks, which reduces the thermal conductivity of the coating and cause better strain tolerability, and hence these defects are considered as an advantage for coating activity [12, 19, 25].

The main reasons for the failure of the TBCs during activity can be the formation of cracks in the BC/TGO or TGO/TC interface, thermal mismatch of TC with the substrate and BC, or occurrence of cracks among the TC structure [7, 11, 12, 26].

The occurrence of thermal shock in coating activity is inevitable, but during it, at a very short time, the coating temperature is reduced about 1000 k; therefore, thermal shock can be the source of many damages in the coating. The furnace method in which the sample is heated inside the furnace to a temperature of about 1100 °C and then quenched in water is one of the best simulations for the thermal shock conditions of the coating [26-28].

In this paper, effect of structure nanonization and compositing on thermal shock behavior of APS YSZ are investigated. In addition, in each case, three different thicknesses have been tested with furnace method to determine the thickness change effect in each case.

## 2. Materials and methods

### 2.1. Materials

In order to check the performance of coatings, 30 mm diameter and 3 mm thick Inconel 738 discs were produced. On the surface of all samples, an Amperit415.006 CoNiCrAlY bondcoat was applied in a thickness of 150 μm. The selected powders to produce the samples' coating are: 8YSZ (Metco 234A-8 %), CYSZ (Metco 205NS) and YSZ-nano (Inframat Sprayable

Nanox™ S4007). All coatings, including topcoat and bondcoat were manufactured using the APS method and Metco 3MB series gun.

### 2.2. Air plasma spraying

Before carrying out spraying process, to increase mechanical bonds between coating and sample, surface of samples blasted with Al<sub>2</sub>O<sub>3</sub> (25 grain mesh). Preheating at 250°C is the next step and then air plasma spraying done with argon and hydrogen as a primary and secondary gases. Detailed parameter of APS process shown in Table 1.

Table 1 plasma spray parameters

Parameter	Unit	YSZ	YSZ-N	CSZ
Current	A	600	600	600
Voltage	V	55	55	55
Primary gas flow (Ar)	nlpm*	40	42	35
Secondary gas flow (H <sub>2</sub> )	nlpm	9	9	9
Carrier gas flow (Ar)	nlpm	2.5	2.5	2.5
Powder feed rate	gr/min	50	40	50
Spray distance	mm	150	150	100
rotation speed	RPM	120	120	120
Surface roughness	μm	0.6 7±0.1	0.67 ±0.1	0.67 ±0.1
Preheat and afterheat temperature	°C	200	200	200

\*: normal liter per minute

Nano-structured and agglomerated YSZ powders need special a range of parameter sets to create nano-structured coating. This range calculated with *critical plasma spray parameters* (CPSP – Eq. (1)) factor and must be between 780 and 1080 [29, 30].

$$CPSP = [Voltage (V) \times Current (A)] / [0.93 \times Primary Argon Gas Flow Rate (nlpm)] \quad (1)$$

After preparing and applying bondcoat to samples, topcoats according to Table 2 created:

Table 2 specification of samples

class	Short code	Thickness (μm)
YSZ (Y) Traditional	D1	300
	D4	450
	D7	600
YSZ-N (YN) Nano-structured YSZ	D10	300
	D13	450
	D16	600
CSZ (C) Compounded YSZ	D19	300
	D22	450
	D25	600

### 2.3. Thermal shock test

Simulation of thermal shock situations was done with the furnace test. The procedure of this test includes: reaching furnace temperature to 1100°C, placing samples into the furnace and waiting for 25min, quenching samples in 20°C water for 5min. The volume of the water is such that its temperature does not change much before and after the quenching. The test is repeated 70 times for all samples unless the sample before the 70th cycle reaches more than 30% of the damage to the coating.

#### 2.4. Coating characterization

At the end of each cycle, photographs were taken from the surface of all samples to determine the amount of degradations of the coating. In addition, before and after the test, Scanning Electron Microscope (SEM) images and Energy-Dispersive Spectrometer (EDS) analysis is taken from the section of samples to check structural changes.

#### 2.5. Calculating coating parameters

In order to quantify the coating behavior, after each cycle, the amount of damage to the coating is determined from its photograph with Digimizer software and shown in Eq. (2).

$$\% D = (\text{damaged area/whole disc area}) \times 100 \quad (2)$$

The best way to compare the performance of different samples in the same cycle is to use a performance factor (PF) that is determined in each cycle using the amount of damage of sample and cycle number (Eq. (3)). The design of this factor is such that

its amount in the initial cycles is around 100 and decreases with the increasing damage of the coating. Since the coating actually operates with 100% of the performance in the starting of application and after damaging, its performance is reduced, so the PF is in good agreement with reality.

$$PF = 10 \times \ln ((\text{end cycle number} / \% D) \times 100) \quad (3)$$

One of the most important factors on coating performance is the thickness of the TGO layer. Since some of the samples are degraded by more than 30% damage before the 70th cycle, in order to compare all the samples, the approximate TGO thickness for all samples in the 70th cycle is calculated. The basis of this calculation is the relation of TGO growth with square root of time [29, 30] and its equation shown in Eq. (4).

$$TGO_{70} = TGO_{ES} \times \sqrt{70/ES} \quad (4)$$

Where  $TGO_{70}$  is the estimated TGO thickness in 70<sup>th</sup> cycle, ES is the end cycle, and  $TGO_{ES}$  is TGO thickness in the end cycle.

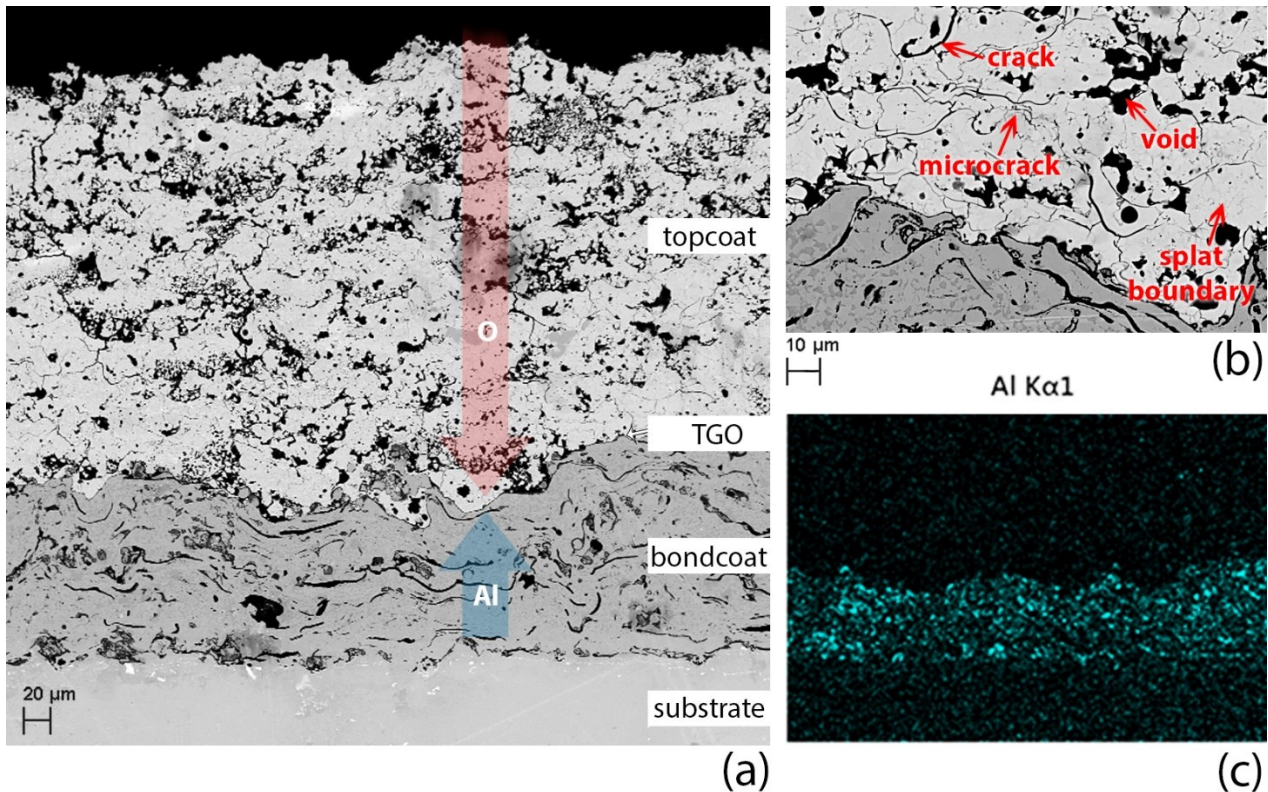


Fig. 1 (a) different layers of a TBC system with YSZ as a topcoat, (b) higher magnification of BC/TC interface and various type of defects and (c) EDS analysis of BC layer and rich area of Al

### 3. Results and discussion

In APS coatings, porosity plays an important role in coating performance in thermal cycles and some of its types are shown in the Fig.1. There are several methods for calculating porosity, which one of them is to convert the cross-sectional image of coating to the binary and calculate the proportion of black pixels to all pixels. Converted image of each class shown in Fig. 2 and

porosity of YSZ, YSZ-N and CSZ are 15.6%, 12.9% and 8.32% respectively. Black pixels represent a variety of imperfections in the coating structure, such as voids, cracks and micro-cracks and so on. YSZ has the highest porosity, but their dispersion is not uniform. Nano-structured YSZ despite its lower porosity, has a more uniform section. Although the CSZ has the least porosity, the horizontal and vertical cracks in its structure are more evident than two other.

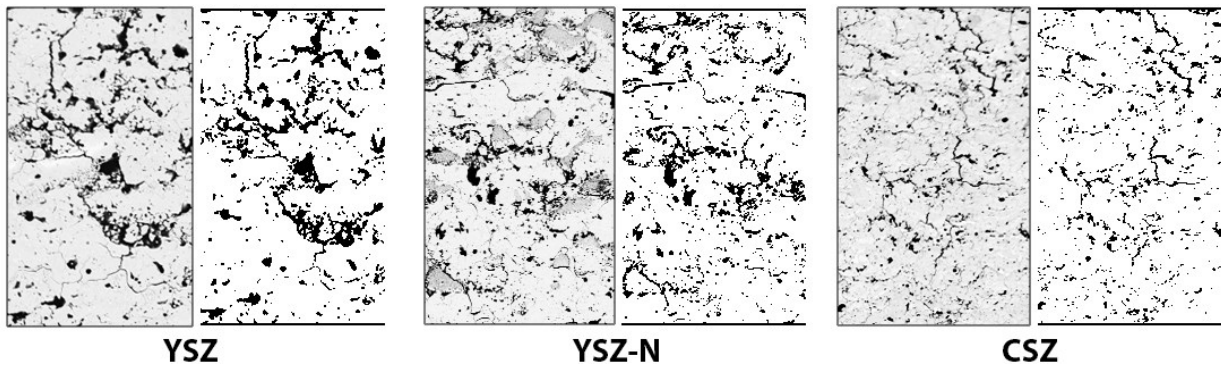


Fig. 2 SEM image and converted to binary format of samples' cross-section

### 3.1. Traditional YSZ

All three samples in the YSZ class endure until the 70th cycle, and their percentage of damage in different cycles was shown in Fig. 3. All curves follow a nearly identical behavior, and they can be seen in three stages:

- Stage One: From the starting of damage to around the 45th cycle where the growth rate is low.
- Stage two: from 45th cycle to around 55th cycle and with a moderate growth rate
- Stage Three: from 55th to 70th cycle and with high growth rates

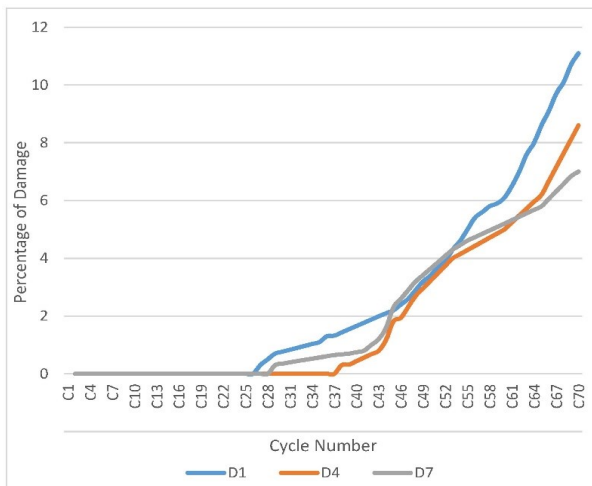


Fig. 3 damage growth diagram for YSZ class

The specific point about these coatings is that with increasing the thickness, the amount of damage decreases and PF increased, that is due to the prolongation of the penetration path of oxygen through the coating defects to BC/TC interface- where the TGO forms. In fact, the TGO needs oxygen for the growth that is supplied from the atmosphere, hence increasing the thickness cause more barriers to oxygen that result is delaying the TGO growth.

Table 3 Details of YSZ class performance

CLASS	SHORTC ODE	%D	SC	EC	TGO <sub>70</sub> (µm)	PF
YSZ (Y)	D1	11	23	70	3.1	64.5
	D4	8.6	22	70	2.8	67
	D7	7	21	70	2.7	69.8

The performance information about this class is given in the

Table 3; the TGO thickness indicates that the majority of the damage occurred within the TGO area. Fig. 4 shows the starting and development of damage in D7. As it can be seen, after the appearance of a vertical crack, the outer part of the coating is completely detached, and any part of the coating is not left on the surface. This behavior, which results from the combination of TGO- and vertical cracks, reveals the role of TGO in damage to YSZ coatings, which is itself due to the high oxygen permeability of this coating.

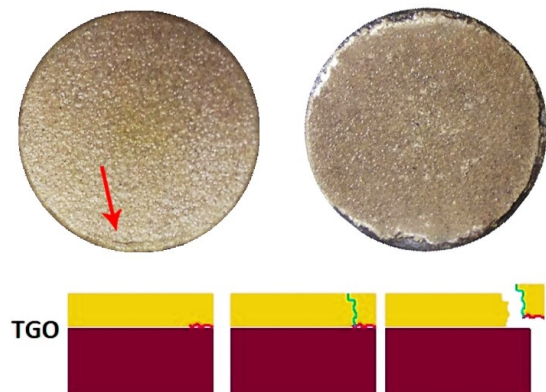
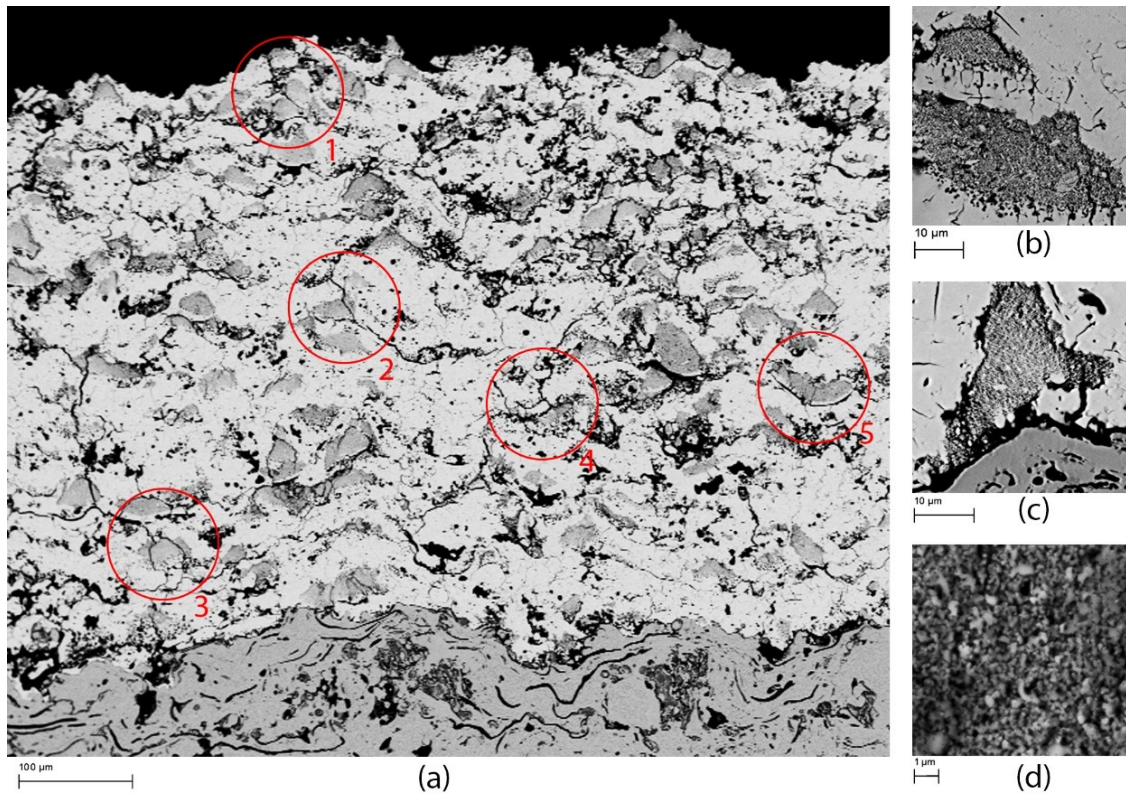


Fig. 4 (a) Starting and growth of damage in the YSZ class and (b) Schematic representation of location and how damage occurred

### 3.2. Nano-structured YSZ

Choosing the right parameters at the spraying time of agglomerated nano-particles caused the non-melted and semi-melted particles will remain in the coating and will be integrated into areas known as nano-zones and their image and more magnifications are shown in Fig. 5. Fairly uniform dispersion of nano-zones at the coating surface indicates proper preparation and right selection of spraying parameters. Since the nano-zones are the only difference of nano- and micro-structured coatings, their behavioral differences can be related to these areas. Nano-zones play different roles in changing the microstructure of the coating, as shown some of them in Fig. 5. Some cracks stop when they reach these areas; some divide into two or more cracks, some attenuate with pass through the nano-zones; some will have to go a longer way, and some will be controlled by these areas. All of these roles (stopping, dividing, dampening, prolonging and controlling) cause closure or prolongation the passage of oxygen through the structure of the coating that resulting in a significant reduction in the thickness of TGO.



**Fig. 5** SEM image of YSZ-N micro-structure, (a) various activities done by the nano-zones: (1) stopping, (2) dividing, (3) dampening, (4) prolonging and (5) controlling, (b), (c) and (d) nano-zone and highest magnification

Damage growth diagram for samples of this class is shown in Fig. 6. In all curves, after the beginning of damage, the graph moves exponentially and with the inclining slope, but around the cycle 52, there is a turning point, and then the slope of the curves is reduced. This is an exceptional behavior that is due to the presence of nano-zones, because in microstructure coatings after the damage occurs, the slope of its progress increases and the operating conditions constantly become worse. Another difference in this class is that with increasing the thickness of the coating its damage became more.

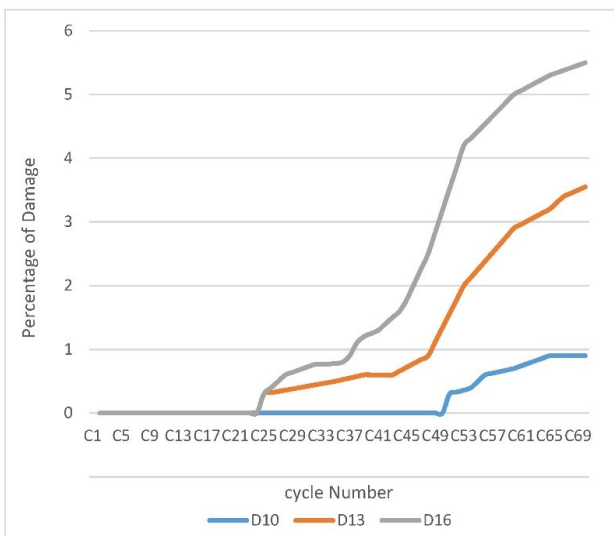


**Fig. 6** damage growth diagram for YSZ-N class

In the YSZ-N class samples, with decreasing the coating

thickness, TGO has increased. This is due to the reduction of the oxygen path from the surface of the coating to the BC/TC interface. Damage in D10 is started in cycle 16, with the removal of a small piece from the edge of the coating, which indicates the growth of crack in the TGO region, but after then it retains its integrity and has not seen any further damage. In the other two cases, the damage type is the same, but the loss of growth has occurred after more damage. Details of YSZ-N class performance shown in Table 4.

**Table 4** Details of YSZ-N class performance

CLASS	SHORT CODE	%D	SC	E C	TGO <sub>70</sub> ( $\mu\text{m}$ )	PF
YSZ-N (YN)	D10	0.9	16	70	1.2	89.6
	D13	3.6	27	70	1.1	75.9
	D16	5.5	31	70	1	71.5

Nano-zones act such as springs in the coating structure and increase the coating's toughness. As a result, reducing the thickness of the coating will increase the toughness and improve the performance of the thermal cycles. Due to the creation of a 0.5-1.0  $^{\circ}\text{C}/\mu\text{m}$  thermal gradient by topcoat, and the ability to withstand against hot corrosion and oxidation, the reduction in thickness of nano-structured coatings is subject to limitations.

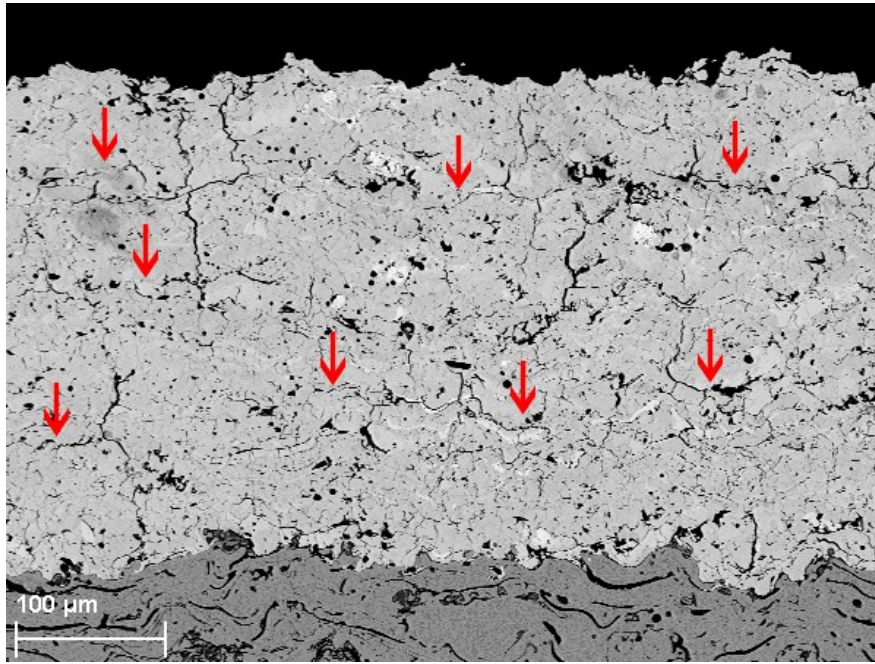


Fig. 7 SEM image of CSZ micro-structure, red arrows shows location of horizontal cracks

### 3.3. CSZ

CSZ has a much denser structure than the other two coatings, with mainly horizontal and vertical cracks in its structure, while the dominant defect in microstructures of YSZ coatings is hollow spaces. Another feature of this coating is the presence of horizontal cracks in different sections, which some of them are shown in the Fig. 7. These cracks during the thermal cycles have the potential to grow, interconnect and form a large horizontal crack, in which case the upper part of the coating is separated and the underside of it, remains on the disk surface. In CSZ coatings, unlike YSZ that damage develops in the TGO region, damage mainly grows through the coating and examples shown in the Fig. 8.



Fig. 8 Samples with CSZ coating after damage

Damage growth diagram for samples with CSZ coating is quite exponentially and after several cycles, the damage is developed with a very high rate that shown in Fig. 9. In this class, similar to the YSZ class, the coating life has been more with increasing the thickness. Regarding the type of damage that is growing horizontal cracks through the coating, it can be concluded that in the initial cycles and during strain tolerances, the horizontal and vertical cracks developed and by joining horizontal and vertical cracks, large parts of the coating are detached.

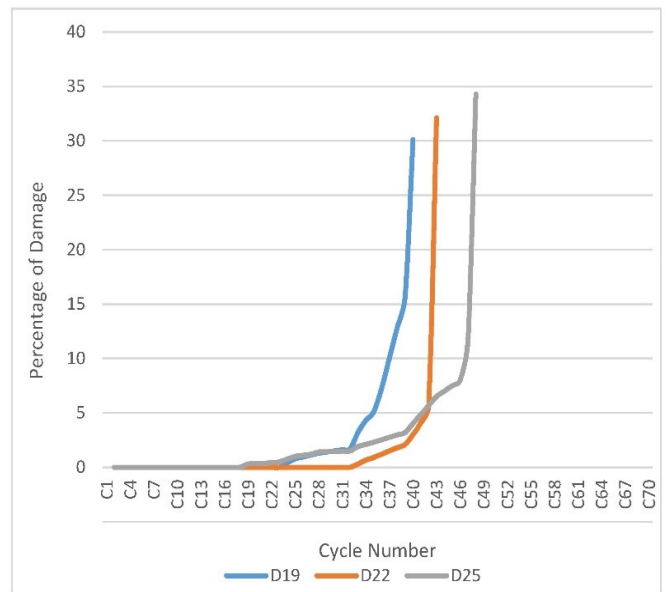


Fig. 9 damage growth diagram for CSZ class

The thickness of TGO in CSZ is less than YSZ (Table 5) and more than YSZ-N. Therefore, the addition of CeO<sub>2</sub> to the YSZ can improve the resistance to oxygen penetration, but the dense structure and horizontal and vertical cracks in this coating have caused other types of damage. The end cycle and the thickness of the TGO in D25, represent the important role of coating thickness on the formation of TGO, but another case in this sample is the starting of damage before other samples. The reason behind this phenomenon is that as coating thickening and with reduction of its toughness, the horizontal cracks grow more rapidly in the middle of the coating, and after joining to a vertical crack, the upper part of the coating is detached.

**Table 5** Details of CSZ class performance

CLASS	SHOR TCODE	%D	SC	EC	TGO 70(μm )	PF
CSZ (C)	D19	30.1	24	40	2.3	48.9
	D22	32.1	33	43	2.2	49
	D25	34.3	19	48	1.9	49.4

**3.4. Comparison of classes**

The starting cycle of damage, sample’s conditions in one of the mid-damage cycles and the state of the samples in the end-cycle

are shown in Fig. 10. The damage type for micro- and nano-structured YSZ is almost similar, and in both classes, there is a good adhesion between the coating and sample surface, but the damage type in the CSZ class is different. In CSZ samples, part of the coating is completely detached from the disk surface, and in some other areas, parts of the coating remain on the surface.

The PF diagram in various cycles is shown in Fig. 11. PF for all samples were nearly 100 before the starting and development of damage, and then the YSZ class was linearly reduced and the reduction in YSZ-N and CSZ classes is exponentially. In the YSZ-N class, the PF of samples in the end cycles is almost constant that is a remarkable behavior, and on the other hand, in the CSZ class, the falling of PF in the end cycles is intense.

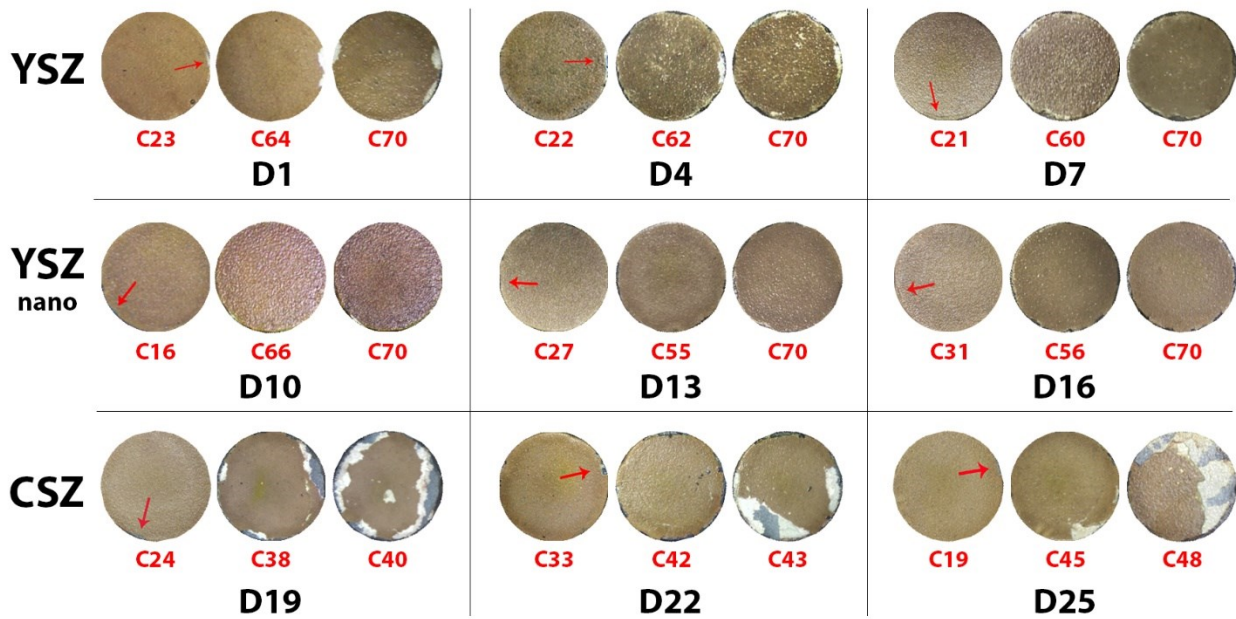


**Fig. 10** starting cycle of damage, one of mid-damage cycles and end-cycle of damage for all samples

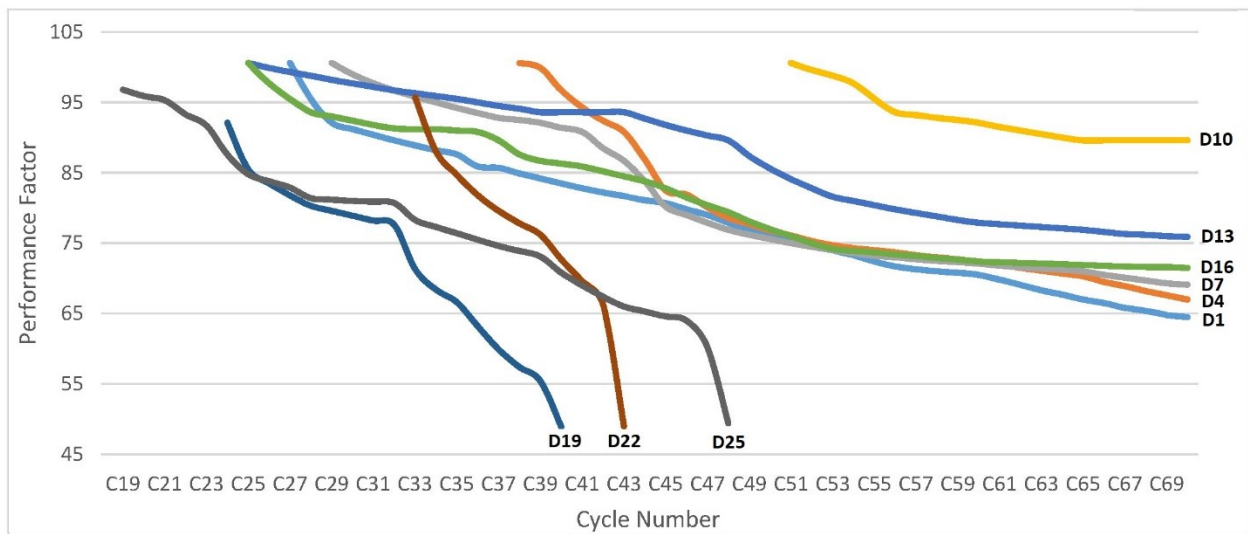


**Fig. 11** Performance factor diagram

The results obtained in this study are consistent with previous studies; for example, Liang [31], Wang [32] and Di Girolamo [33] were showed that the durability of nano-structured YSZ coatings in thermal shock conditions is more than three times the

conventional YSZ coating. In some other references such as [34] [35] [36], the properties of CSZ in TBCs have been investigated, whose results are in good agreement with the results of this paper.

#### 4. Conclusions

The performance of YSZ based thermal barrier coatings, conventional microstructure YSZ, nano-structured YSZ and compounded YSZ (CSZ) in thermal shock conditions has been investigated. In each class, samples with thickness of 300, 450 and 600  $\mu\text{m}$  was produced; the furnace method was used for thermal shock testing, and test was repeated 70 times. The results showed that behavior of conventional YSZ is almost linear and its damage mainly occurs throughout the TGO region. In these samples, the thickness of TGO is high, which indicates the high oxygen permeability of this material. In addition, with the increase in thickness of this class, performance has improved. Nano-structured YSZ coatings exhibit the best performance, and the amount of damage and thickness of TGO are very low. Furthermore, in these samples, with increasing the damage, the slope of grows has decreased, which is a significant phenomenon. In this class, the lower thickness has shown better performance. CSZ class coatings have a denser structure than two other classes, and in their microstructure, there are many horizontal cracks that lead development of damage among the topcoat and then separating its upper part. In general, CSZ coatings did not provide acceptable behavior, but its performance with increasing thickness slightly improved.

#### 5. Acknowledgement

The authors thank Mapna Turbine Blade Eng. & Mfg. co. PARTO, for experimental support throughout this study.

#### 6. References

- [1] T. Steinke, D. Sebold, D. E. Mack, R. Vaßen, and D. Stöver, "A novel test approach for plasma-sprayed coatings tested simultaneously under CMAS and thermal gradient cycling conditions," *Surface and Coatings Technology*, vol. 205, no. 7, pp. 2287-2295, 12/25/ 2010.
- [2] B. A. Pint, I. G. Wright, and W. J. Brindley, "Evaluation of thermal barrier coating systems on novel substrates," (in English), *Journal of Thermal Spray Technology*, vol. 9, no. 2, pp. 198-203, 2000/06/01 2000.
- [3] S. Sampath, U. Schulz, M. O. Jarligo, and S. Kuroda, "Processing science of advanced thermal-barrier systems," *MRS Bulletin*, vol. 37, no. 10, pp. 903-910, 2012.
- [4] J. Smith *et al.*, "Thermal Barrier Coating Validation Testing for Industrial Gas Turbine Combustion Hardware," *Journal of Engineering for Gas Turbines and Power*, vol. 138, no. 3, p. 031508, 2016.
- [5] A. Bolcavage, A. Feuerstein, J. Foster, and P. Moore, "Thermal shock testing of thermal barrier coating/bondcoat systems," *Journal of Materials Engineering and Performance*, vol. 13, no. 4, p. 389, 2004.
- [6] G. Di Girolamo, C. Blasi, A. Brentari, and M. Schioppa, "Microstructure and thermal properties of plasma-sprayed ceramic thermal barrier coatings," 2013.
- [7] B. Saeedi, A. Sabour, and A. Khoddami, "Study of microstructure and thermal shock behavior of two types of thermal barrier coatings," *Materials and corrosion*, vol. 60, no. 9, pp. 695-703, 2009.
- [8] S. E. Hosseinidoost, A. Sattari, M. Eskandari, D. Vahidi, P. Hanafizadeh, and P. Ahmadi, "Techno-Economy Study of wind energy in Khvaf in Razavi Khorasan Province in Iran," *Journal of Computational Applied Mechanics*, vol. 47, no. 1, pp. 53-66, 2016.
- [9] M. Hamed and H. Eisazadeh, "Numerical Simulation of Nugget Geometry and Temperature Distribution in Resistance Spot Welding," *Journal of Computational Applied Mechanics*, vol. 46, no. 1, pp. 13-19, 2015.
- [10] M. Hamed and A. Farzaneh, "Optimization of Dimensional Deviations in Wax Patterns for Investment Casting," *Journal of Computational Applied Mechanics*, vol. 45, no. 1, pp. 23-28, 2014.
- [11] G. Moskal, "Thermal barrier coatings: characteristics of microstructure and properties, generation and directions of development of bond," *Journal of Achievements in Materials and Manufacturing Engineering*, vol. 37, no. 2, pp. 323-331, 2009.
- [12] N. P. Pature, M. Gell, and E. H. Jordan, "Thermal barrier coatings for gas-turbine engine applications," *Science*, vol. 296, no. 5566, pp. 280-284, 2002.
- [13] D. Yang, Y. Gao, H. Liu, and C. Sun, "Thermal shock resistance of bimodal structured thermal barrier coatings by atmospheric plasma spraying using nanostructured partially stabilized zirconia," *Surface and Coatings Technology*, vol. 315, pp. 9-16, 2017/04/15/ 2017.
- [14] M. G. Gok and G. Goller, "Microstructural characterization of GZ/CYSZ thermal barrier coatings after thermal shock and CMAS+hot corrosion test," *Journal of the European Ceramic Society*, vol. 37, no. 6, pp. 2501-2508, 2017/06/01/ 2017.
- [15] X. Guo, Z. Lu, Y.-G. Jung, L. Li, J. Knapp, and J. Zhang, "Thermal Properties, Thermal Shock, and Thermal Cycling Behavior of Lanthanum Zirconate-Based Thermal Barrier Coatings," *Metallurgical and Materials Transactions E*, journal article vol. 3, no. 2, pp. 64-70, June 01 2016.
- [16] H. Jamali, M. Loghman-Estarki, R. S. Razavi, R. Mozafarinia, H. Edris, and S. Bakhshi, "COMPARISON OF THERMAL SHOCK BEHAVIOR OF NANO-7YSZ, 15YSZ AND 5.5 SYSZ THERMAL BARRIER COATINGS PRODUCED BY APS METHOD," *Ceramics-Silikáty*, vol. 60, no. 3, pp. 210-219, 2016.
- [17] W. Chi, S. Sampath, and H. Wang, "Microstructure-Thermal Conductivity Relationships for Plasma-Sprayed Ytria-Stabilized Zirconia Coatings," *Journal of the American Ceramic Society*, vol. 91, no. 8, pp. 2636-2645, 2008.
- [18] R. Vaßen, M. O. Jarligo, T. Steinke, D. E. Mack, and D. Stöver, "Overview on advanced thermal barrier coatings," *Surface and Coatings Technology*, vol. 205, no. 4, pp. 938-942, 11/15/ 2010.
- [19] N. Curry, N. Markocsan, X.-H. Li, A. Tricoire, and M. Dorfman, "Next generation thermal barrier coatings for the gas turbine industry," *Journal of thermal spray technology*, vol. 20, no. 1-2, pp. 108-115, 2011.
- [20] R. Vaßen, F. Traeger, and D. Stöver, "New Thermal Barrier Coatings Based on Pyrochlore/YSZ Double-Layer Systems," *International Journal of Applied Ceramic Technology*, vol. 1, no. 4, pp. 351-361, 2004.
- [21] X. Cao, R. Vassen, and D. Stoeber, "Ceramic materials for thermal barrier coatings," *Journal of the European Ceramic Society*, vol. 24, no. 1, pp. 1-10, 2004.
- [22] Y. Zeng, S. W. Lee, L. Gao, and C. X. Ding, "Atmospheric plasma sprayed coatings of nanostructured zirconia,"

- Journal of the European Ceramic Society*, vol. 22, no. 3, pp. 347-351, 3// 2002.
- [23] R. S. Lima and B. R. Marple, "Thermal Spray Coatings Engineered from Nanostructured Ceramic Agglomerated Powders for Structural, Thermal Barrier and Biomedical Applications: A Review," (in English), *Journal of Thermal Spray Technology*, vol. 16, no. 1, pp. 40-63, 2007/03/01 2007.
- [24] S. Tamaddon Masoule, Z. Valefi, N. Ehsani, and H. Qazi Lavasani, "Thermal Insulation and Thermal Shock Behavior of Conventional and Nanostructured Plasma-Sprayed TBCs," *Journal of Thermal Spray Technology*, journal article vol. 25, no. 8, pp. 1684-1691, December 01 2016.
- [25] M. O. Jarligo, D. E. Mack, R. Vassen, and D. Stöver, "Application of plasma-sprayed complex perovskites as thermal barrier coatings," *Journal of Thermal Spray Technology*, vol. 18, no. 2, pp. 187-193, 2009.
- [26] R. A. Miller, "Thermal barrier coatings for aircraft engines: History and directions," *Journal of Thermal Spray Technology*, vol. 6, no. 1, pp. 35-42, 1997.
- [27] C.-B. Liu, Z.-M. Zhang, X.-L. Jiang, L. Min, and Z.-H. Zhu, "Comparison of thermal shock behaviors between plasma-sprayed nanostructured and conventional zirconia thermal barrier coatings," *Transactions of Nonferrous Metals Society of China*, vol. 19, no. 1, pp. 99-107, 2009.
- [28] M. Rahnavard, M. Ostad Ahmad Ghorabi, M. Rahnein, and H. Rafiee, "Effects of incorporation of micro and nano Al<sub>2</sub>O<sub>3</sub> layers on thermal shock behaviour of YSZ thermal barrier coatings," *Canadian Metallurgical Quarterly*, vol. 55, no. 3, pp. 312-320, 2016.
- [29] E. P. Song, J. Ahn, S. Lee, and N. J. Kim, "Microstructure and wear resistance of nanostructured Al<sub>2</sub>O<sub>3</sub>-8wt.%TiO<sub>2</sub> coatings plasma-sprayed with nanopowders," *Surface and Coatings Technology*, vol. 201, no. 3-4, pp. 1309-1315, 10/5/ 2006.
- [30] H. Huang, C. Liu, L. Ni, and C. Zhou, "Evaluation of TGO growth in thermal barrier coatings using impedance spectroscopy," *Rare Metals*, vol. 30, pp. 643-646, 2011.
- [31] B. Liang and C. Ding, "Thermal shock resistances of nanostructured and conventional zirconia coatings deposited by atmospheric plasma spraying," *Surface and Coatings Technology*, vol. 197, no. 2, pp. 185-192, 2005.
- [32] W. Wang, C. Sha, D. Sun, and X. Gu, "Microstructural feature, thermal shock resistance and isothermal oxidation resistance of nanostructured zirconia coating," *Materials Science and Engineering: A*, vol. 424, no. 1, pp. 1-5, 2006.
- [33] G. Di Girolamo, F. Marra, C. Blasi, E. Serra, and T. Valente, "Microstructure, mechanical properties and thermal shock resistance of plasma sprayed nanostructured zirconia coatings," *Ceramics International*, vol. 37, no. 7, pp. 2711-2717, 2011.
- [34] M. Nejati, M. Rahimipour, and I. Mobasherpour, "Evaluation of hot corrosion behavior of CSZ, CSZ/micro Al<sub>2</sub>O<sub>3</sub> and CSZ/nano Al<sub>2</sub>O<sub>3</sub> plasma sprayed thermal barrier coatings," *Ceramics International*, vol. 40, no. 3, pp. 4579-4590, 2014.
- [35] M. Habibi and S. Guo, "The hot corrosion behavior of plasma sprayed zirconia coatings stabilized with yttria, ceria, and titania in sodium sulfate and vanadium oxide," *Materials and Corrosion*, vol. 66, no. 3, pp. 270-277, 2015.
- [36] S. Park, J. Kim, M. Kim, H. Song, and C. Park, "Microscopic observation of degradation behavior in yttria and ceria stabilized zirconia thermal barrier coatings under hot corrosion," *Surface and Coatings Technology*, vol. 190, no. 2, pp. 357-365, 2005.